International Journal of Computing and Digital Systems
ISSN (2210-142X)
Int. J. Com. Dig. Sys. 9, No.3 (May-2020)

http://dx.doi.org/10.12785/ijcds/090314

Investigating the Visibility of 28 and 73 GHz Frequency Bands for Outdoor MIMO Channel

Alauddin Al-Omary[1]

[1] *College of IT, University of Bahrain, Kingdom of Bahrain*

Received 12 Nov. 2019, Revised 30 Jan. 2020, Accepted 13 Apr. 2020, Published 1 May 2020

Abstract: As the world moves toward 5G networks, the wireless spectrum below 6 GHz will not meet future 5G network needs. Several new bands need to be investigated to check their characteristics and usability for future networks. In this paper, the investigation of outdoor performance of Multiple Input Multiple Output (MIMO) systems for 28 GHz and 73 GHz frequency bands is explored. A realistic scenario based on Statistical Spatial Channel Model (SSCM) over frequency selective Rayleigh fading channel is used in simulating MIMO channel. The channel performance is predicted for different propagation scenario, different combination of MIMO transmitter and receiver antennas and different antenna separation distances. Many parameters are computed, analyzed and compared to examine the MIMO performance for these frequencies. This includes the channel path loss, the received power, directional and Omni-directional Power Delay Profile (PDP), Angle of departure (AoD) and Angle of Arrival (AoA) power spectrum. The investigation of 28 GHz and 73 GHz frequencies is helpful in revealing the main features of the new frequency bands, their mmWave system-wide behavior, their maximum coverage distance as well as their usage visibility. The investigated frequencies are expected to be used in the first deployment of the 5G networks.

Keywords: mm-Wave, 28 GHz, 73 GHz, MIMO, Statistical Spatial Channel Model (SSCM), 5G Networks

1. INTRODUCTION

Recently, the research on 5th Generation (5G) networks witnessed significant and intensified efforts to examine the enabling technologies that can be used to implement the 5G network. The motivation behind 5G network is triggered by the massive growth of global subscriptions and the huge requirement for new services. Video is expected to dominate the total mobile traffic volume and has already presented significant challenges to mobile networks. Some applications like Virtual Reality (VR) is expected to need at least 10Gbps. 5G is an advanced evolution of 4G networks that will link our physical, virtual and social worlds. The key requirement for 5G is to increase the capacity 1000 to "10000-time". This can be done by increasing network density, spectrum efficiency, and spectrum extension. High network density can be achieved by using small cells. Spectrum efficiency can be increased using massive MIMO and spectrum extension can be achieved using mmWave spectrum [1-5]. As the demand for more bandwidth is increasing, the massive spectrum available between 6 and 300 GHz is an attractive solution. Several mmWave bands are currently being considered for global 5G networks. The 28- and 73-GHz frequency bands for outdoor communications are relevant, as the attenuation loss induced from atmospheric absorption is minor over a realistic mmWave cell radius of 200 m [1]. Moreover, the Federal Communications Commission has recently issued new rulemakings to bring these bands into service [2], [3]. Extensive studies are necessary to determine coverage distances, path loss, and system configurations for mmWave wireless communications networks that will operate on 28 and 73 GHz. In this paper, the performance of Multiple Input Multiple Output (MIMO) systems for 28 GHz and 73 GHz frequency is investigated. This paper is an extension of the previous published work [6] in ICONCS 2018 conference. More simulation scenarios had been considered and many parameters are calculated and compared to investigate the MIMO performance for these frequencies. These parameters include: Path loss, Received power, Directional and Omni-directional Power Delay Profile (PDP), Angle of departure (AoD) power spectrum, Angle of Arrival (AoA) power spectrum. Moreover, different realistic scenarios that cover many aspects of MIMO system using the proposed channel models are conducted. These include simulation using various numbers of transmitted and received antenna, different types of antennas, several separation distance between transmitters and receivers, and different transmission environments. The results are analyzed, and a conclusion was drawn about the main characteristics and usability of these ultra-high frequencies.

E-mail: aalomary@uob.edu.bh

The rest of the paper is organized as follows. Section 2 presents the literature review. In section 3, the scope of the paper is illustrated. Section 4 describe the Statistical Spatial Channel Model (SSCM). Section 5 outlines the simulation scenario. In Section 6 we evaluate and discuss the results. Finally, we summarize our contributions and draw conclusions.

2. LITERATURE REVIEW

By the end of year 2020, the volume of data is expected to exceed 1,000 times of the data that is currently available as was predicted by Ericsson [2]. Similarly, the Universal Mobile Telecommunication System (UMTS) predicted that mobile data traffic could exceed 800 Mbps/subcarrier by the year 2020 [4]. Fundamental changes in system and network design need to be done to cope with this traffic growth. The new 5G network aimed to make revolutionary change in network speed, latency, bandwidth, and energy consumption. The potential of new spectrum such as millimeter-wave (mmWave) frequencies, had been investigated by [3], [4] and [6]. Channel characterization at both mmWave and centimeter-wave (cmWave) bands has been conducted by many previous research papers. Samsung who recognize the feasibility of mmWave for access in cellular systems [5] proposed one of the first studies of using mmWave as a key component for cellular 5G networks. In [7] outdoor access scenarios based on propagation measurements at 28, 38, 60 and 73 GHz are introduced. In [8], researchers studied the effectiveness of beamforming and Multi User MIMO in mmWave bands for system rate improvements. Researchers at [9] proposed the concept of mmWave networks overlaying to convert small-cells to larger macro-cells. This concept is one of the model system architecture of current 5G standards. The authors in [10-12] studied and modeled the Urban Microcellular (UMi) and indoor channels at 28 GHz and 60 GHz. It is very likely that 28 GHz will be used for the first 5G deployments in South Korea, US and Japan. Beside that 28 GHz, 38 GHz, 60 GHz and 73 GHz are strong candidate bands for the 5G networks [1], [3]. As shown in figure (1), the 28- and 73-GHz frequency bands for outdoor communications have advantages of less attenuation loss induced from atmospheric absorption when compared with other ultra-high bands (20, 38 and 60 GHz). The absorption loss is known to have a peak at around 60 GHz and a small "notch" at around 30 GHz. It was reported that targeted bands especially the 28 GHz one has attenuation loss of less than 0.1 dB over a realistic mmWave cell radius of 200 m [13-14] while it is significantly higher at 60 GHz (~4 dB/200 m).

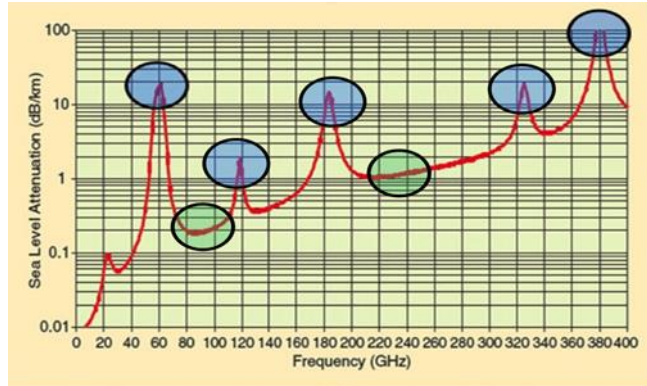

Figure 1. Air attenuation at sea level versus frequency[1]

3. CHANNEL MODEL

Two kinds of channel models, namely, correlation-based stochastic models (CBSMs) and geometry-based stochastic models (GBSMs) are widely used to evaluate the performances of the wireless communication systems. Because of its low complexity, CBSMs is mainly used for analyzing the theoretical performance of MIMO systems. The accuracy of CBSMs is also limited for the realistic MIMO system and it is difficult to model wireless channels considering the non-stationary phenomenon and spherical wave effects. In contrast, the GBSMs model has higher computation complexity but it has higher accuracy, can accurately reflect the realistic channel properties, and is more suitable for massive MIMO channel.

3.1 Statistical Spatial Channel Model

In this paper, a GBSMs model channel was used. This is because the GBSMs models are very useful because with this model one can isolate the effect of antennas from the actual propagation characteristics. They also allow making analysis with different antenna configurations, elements, polarizations etc. together with beamforming and so on. The geometry-based models have much better physical meaning, which makes it easier to analyze the results against any possible scenario. A GBSM-like developed at New York university [15-18] called the Statistical Spatial Channel Model (SSCM) is used to model the MIMO channel. SSCM is a multi-frequency 3-dimensional (3-D) measurement-based Channel Impulse Response (CIR) model [15]. Like the 3GPP channel model SSCM supports arbitrary carrier frequency, RF bandwidth, and antenna beam width for both omnidirectional and arbitrary directional antennas. SSCM have been used successfully in modelling mmWave channels [13]. It utilizes time clusters (TC) and spatial lobes (SL) to model the omnidirectional CIR and corresponding joint angle of departure (AoD)/angle of arrival (AoA) power spectra. Time clusters are composed of multipath components (MPCs) traveling closely in

[1] Samimi, M., et al., "28 GHz Angle of Arrival and Angle of Departure Analysis for Outdoor Cellular Communications using Steerable Beam Antennas in New York City," in the 2013 IEEE Vehicular Technology Conference (VTC), June 2-5, 2013.

time. MPCs arrive from potentially different angular directions in a short excess delay time window. Spatial lobes represent main directions of arrival (or departure) where energy arrives over several hundreds of nanoseconds. Multiple paths within a TC can arrive at unique pointing angles [13] and can be detected due to high gain directional antennas. As was reported in [13], the time cluster spatial lobe (TCSL) approach implements a physically-based clustering scheme (e.g., the use of a fixed inter-cluster void interval representing the minimum propagation time between likely reflection or scattering objects). It was derived from field observations and can be used to extract TC and SL statistics for any ray tracing or measurement data sets [13]. The time-partitioning methodology delineates the beginning and end times of each time cluster, using a 25ns minimum inter-cluster void interval. Sequentially arriving MPCs that occur within 25 ns of each other are assumed to belong to one TC.

The double-directional omnidirectional CIR is commonly used to represent the radio propagation channel between a transmitter and receiver, and can be expressed as in eq. (1) [13], [18]:

$$h_{omni}\,(t,\Theta,\phi) = \sum_{n=1}^{N}\sum_{m=1}^{Mn} a_{m,n}\ e^{j\varphi_{m,n}}\ \delta\left(t - \tau_{m,n}\right)\ \delta\left(\Theta - \Theta_{m,n}\right)\ \delta\left(\phi - \phi_{m,n}\right) \quad (1)$$

Where t denotes absolute propagation time, $\Theta = (\boldsymbol{\theta}, \boldsymbol{\phi})_{Tx}$, and $\phi = (\boldsymbol{\theta}, \boldsymbol{\phi})_{Rx}$ are the vectors of azimuth/elevation AoDs and AoAs, respectively. N and Mn denotes the number of time clusters (defined in [17]), and the number of cluster subpaths, respectively. $a_{m,n}$ is the amplitude of the mth subpath belonging to the nth time cluster; $\varphi_{m,n}$ and $\tau_{m,n}$ are the phases and propagation time delays, respectively; $\Theta_{m,n}$ and $\phi_{m,n}$ are the azimuth/elevation AODs, and azimuth/elevation AoAs, respectively, of each multipath component.

The joint AoD-AoA power spectra $P(\Theta,\phi)$ in 3-D can be obtained by integrating the magnitude squared of (1) over the propagation time dimension,

$$P(\Theta,\phi) = \int_0^{\infty} |h(t,\Theta,\phi)|^2\, dt \quad (2)$$

$$P(\Theta,\phi) = \sum_{n=1}^{N}\sum_{m=1}^{Mn} |a_{m,n}|^2\ \delta\left(\Theta - \Theta_{m,n}\right)\ \delta\left(\phi - \phi_{m,n}\right) \quad (3)$$

The directional Power delay profile (PDP) at a desired Tx-Rx unique antenna-pointing angle, and for arbitrary Tx and Rx antenna patterns can be obtained by partitioning the omnidirectional CIR to yield,

$$h_{dir}\,(t,\Theta_d,\phi_d) = \sum_{n=1}^{N}\sum_{m=1}^{Mn} a_{m,n}\ e^{j\varphi_{m,n}}\ \delta\left(t - \tau_{m,n}\right) g_{TX}\left(\Theta_d - \Theta_{m,n}\right)\ g_{RX}\left(\phi_d - \phi_{m,n}\right) \quad (4)$$

Where (Θ_d, ϕ_d) are the desired Tx-Rx antenna pointing angles, $g_{TX}(\Theta)$ and $g_{RX}(\phi)$are the arbitrary 3-D (azimuth and elevation) Tx and Rx complex amplitude antenna patterns of multi-element antenna arrays, respectively. The directional PDP is obtained in eq. (4) by amplifying the power levels of all multipath components lying close to the desired pointing direction. The power levels of multipath components lying far away from the desired pointing direction is set to 0 [18].

3.2 Path Loss Model

In this paper, the close-in free space reference distance (CI) path loss model with a 1 m reference distance is used [20-23]. The path loss is expressed as:

$$PL^{CL}\,(f,d)[dB] = FSPL\,(f,1m)[dB] + 10n\log_{10}(d) + AT[dB] + X_{\sigma}^{CL} \quad (5)$$

$$\text{Where d} \geq 1\text{m}$$

where f denotes the carrier frequency in GHz, d is the 3D T-R separation distance, n represents the path loss exponent (PLE), AT is the attenuation term induced by the atmosphere, $X_{\sigma}^{CL}$is a zero-mean Gaussian random variable with a standard deviation σ in dB. *FSPL (f, 1m)* denotes the free space path loss in dB at a T-R separation distance of 1 m at the carrier frequency f:

$$FSPL(f,1m)[dB] = 20\,\log_{10}\left(\frac{4\pi f \times 10^9}{c}\right) = 32.4[db] + 20\,\log_{10}(f) \quad (6)$$

Where c is the speed of light in vacuum, and f is in GHz. The term AT is characterized by:

$$AT[dB] = \alpha\,[dB\,/m] \times d\,[m] \quad (7)$$

where α is the attenuation factor in $dB\,/m$ for the frequency range of 1 GHz to 100 GHz, which includes the collective attenuation effects of dry air (including oxygen), water vapour, rain, and haze [21]. The parameter d is the 3D T-R separation distance used in (5).

4. SIMULATION METHODS AND PARAMETERS

The channel behavior of the two mmWave bands (28GHz and 73 GHz) was studied using NYUSIM simulator [24]. NYUSIM is a MATLAB-based

statistical simulator that can be used to generate realistic temporal and spatial channel responses to support realistic physical- and link-layer simulations and design for fifth-generation (5G) cellular communications. NYUSIM is built upon the statistical spatial channel model [18] for broadband millimeter-wave (mmWave) wireless communication systems developed by researchers at New York University (NYU).

4.1 Simulation Environment

Let us assume a single-cell single-user MIMO system operating at mmWave bands within RF bandwidth of 800 MHz in the in UMi scenario. The base station is equipped with different antenna elements comprising two types of antenna Uniform Linear Antenna (ULA) and Uniform Rectangular Antenna (URA). The user has also same antenna types. Signal-to-noise ratios (SNRs) are fixed at certain values.

4.2 Simulation Scenario

We investigate the outdoor MIMO performance for 28 GHz and 73 GHz frequency bands. Different realistic scenarios that cover many aspects of MIMO system using the proposed channel models are conducted. These include simulation using various numbers of transmitted and received antenna, different types of antennas, several separation distance between transmitters and receivers, and different transmission environments as shown below:

1. Transmitter is set to (16, 32, 64) and receiver is set to (1, 4, 8) respectively.
2. Two types of antenna are used, Uniform Linear Array (ULA) and square shape Uniform Rectangular Array (URA).
3. Two hundred random channel realizations were performed with distances between transmitter and receiver ranging from 50 to 500m (50, 100, 150, 200, 250, 300, 350, 400, 450, 500 m).
4. Two types of Transmission environment are investigated Line of Sight (LOS) and None Line of Sight (NLOS).

The following parameters are calculated and compared for each of the above-mentioned cases:

a. Path loss (as was expressed in eq. 5)
b. Path loss exponent (determines how quickly the Received Signal Strength (RSS) falls with distance).
c. Coverage distance
d. Directional Power delay profile (PDP) with strongest power,
e. Omni-directional PDP
f. Angle of departure (AoD) power spectrum
g. Angle of Arrival (AoA) power spectrum

4.3 Simulation parameters

The following input parameters settings were used to run a simulation:

4.3.1 Fixed parameters

- Base station antenna height: 25 m
- RF bandwidth: 800 MHz
- Scenario: UMi
- Tx Power: 30 dBm
- Barometric Pressure: 1013.25 mbar
- Humidity: 50%
- Temperature: 20 ^{o} C
- Rain Rate: 0 mm/hr
- Polarization: Co-Pol
- Foliage Loss: No
- Tx Antenna Spacing: 0.5 wavelength
- Rx Antenna Spacing: 0.5 wavelength
- Tx Antenna Azimuth HPBW: 10.9^{o} for ULA and 7° for URA
- Tx Antenna Elevation HPBW: 8.6^{o} for ULA and 7° for URA
- Rx Antenna Azimuth HPBW: 10.9^{o} for ULA and 7° for URA
- Rx Antenna Elevation HPBW: 8.6^{o} for ULA and 7° for URA

The variable simulation parameters are shown in table

TABLE 1. THE VARIABLE SIMULATION PARAMETERS

Frequency	**28Ghz**						**73GHz**					
No of Tx Antenna	16		32		64		16		32		64	
No of Rx Antenna	1		4		8		1		4		8	
Distance between Tx and Rx	50-500m		50-500m		50-500m		50-500m		50-500m		50-500m	
Environment	LoS	NLoS	LoS	NLoS	LoS	NLoS	LoS	NLoS	LoS	NLoS	LoS	NLoS
Antenna Type	ULA	URA	ULA	URA	ULA	URA	ULA	URA	ULA	URA	ULA	URA
No of locations for receivers	10 locations											
No of rounds	20 rounds for each location											

5. SIMULATION RESULTS AND DISCUSSION

The parameters mentioned in section 4.1 were calculated. These parameters are evaluated to draw conclusion about the performance of MIMO system for 28 GHz and 73 GHz bands.

5.1 Coverage distance

In order to investigate the allowable coverage distance for 28 GHz and 73 GHz frequency bands, many simulation rounds are conducted using different separation distances between Transmitter and receiver (50-1000m). Besides that, the simulation round is done using different propagation scenarios and different antennas. Coverage implies there is enough signal strength. Table (2) shows the different dBm signal strength and their signal status. It is obvious from the table that -60 dBm is good reliable signal and -67 dBm is the minimum for voice and non-HD video signal[2].

Table (3) shows the summary results of received power (P_r) in dBm for 500m. The 500 m distance is critical because beyond this value the received power in some cases will drop below – 60 dBm, which is considered as, nearly perfect value of received power.

From table (3) we can notice the following cases:

Case 1: Using LOS the 500-coverage distance for both 28 GHz and 73 GHz is guaranteed and even can be increased little more beyond 500m. This is true for both ULA and URA antennas.

Case 2: Using NLOS the received power for 28 GHz frequency is still good for URA antenna but for ULA antenna all the received power is slightly less than -60dBm but it is still within the acceptable range and can be detected so the 500-coverage area could be ok for 28GHz.

Case 3: Using NLOS, for 73 GHz all the received power will be less than -60 dBm by different margin using ULA or URA antenna and 500m-coverage could be risky.

TABLE 2. SIGNAL STRENGTH (DBM) AND THEIR SIGNAL STATUS[3]

Received Signal power strength	Signal status
-30 dBm	Perfect signal
-50 dBm	Excellent signal
-60 dBm	Good reliable signal
-67 dBm	Minimum for Voice and non-HD signal
-70 dBm	Light browsing and email
-80 dBm	Unstable signal

TABLE 3. RECEIVED POWER FOR DIFFERENT FREQUENCIES AND MIMO SCENARIO FOR 500 M T-R DISTANCE

Frequency	MIMO Antenna	*Pr* in dBm (LOS) / ULA	*Pr* in dBm (LOS) / URA	*Pr* in dBm (NLOS) / ULA	*Pr* in dBm (NLOS) / URA
28 GHz	16X1	-43.1	-38.5	-70.2	-63.2
	32X4	-37.2	-33.3	-68.1	-57.3
	64X8	-34	-31.2	-66.3	-53.1
73GHz	16X1	-53.3	-48.5	-75.1	-70.3
	32X4	-48.7	-45.1	-72.2	-68.2
	64X8	-42.3	-40.6	-71.4	-65.4

[2] https://www.cisco.com/c/en/us/td/docs/solutions/Enterprise/Borderless_Networks/Unified_Access/CMX/CMX_RFFund.pdf

[3] https://powerfulsignal.com/cell-signal-strength/, and https://eyesaas.com/wi-fi-signal-strength/

TABLE 4. AOD, AOA, RECEIVED POWER AND R.M.S DELAY SPREAD FOR 32X4 ANTENNA, 28GHZ, 300M

beam#	Time Delay (ns)	Received Power (dBm)	Phase (rad)	Azimuth AoD (degree)	Elevation AoD (degree)	Azimuth AoA (degree)	Elevation AoA (degree)	Path Loss (dB)	R.M.S Delay Spread (ns)
1	1003	-39.3	5.9	5	-14	194.2	13	111.1	7.1
2	1005	-40.2	5.2	17	-17.8	186.4	13	110.4	6.4
3	1008	-37.4	4	5	-13.6	192.9	16	110.4	7.1
4	1011	-60.2	4.3	4	-14.8	171.6	12	124.1	11.2
5	1013	-33.6	4	12	-15.6	196.2	10	113.4	2.3
6	1070	-87.6	0.6	360	-15	190.4	17	111.4	1.9
7	1073	-85	0.8	357	-15.1	187.3	18	109.9	1.4
8	1077	-115.4	2	14	-17.9	209.4	21	123.1	15.1
9	1081	-115.4	1.4	11	-15.9	188.7	29	121.8	11.8
10	1084	-117.6	5.5	355	-13.2	210.2	34	118.3	1.8
11	1086	-64.1	1.4	357	-14.9	201.1	27	114	1.3
12	1089	-66.1	1.5	21	-12.7	197.7	12	118.3	9.8
13	1090	-68.7	3.6	359	-18.5	175.9	14	120.8	6.6
14	1039	-128.8	4.2	13	-13.6	180.8	12	114.9	17.7
15	1042	-129.6	0.1	28	-14.7	184.6	6	123.9	12.9
16	1108	-130.3	6	20	-15.4	190.6	1	132.7	34.3
17	1110	-108.3	5.1	17	-12.5	210.1	25	128.7	45.8
18	1113	-107.4	0.9	4	-12.5	203.8	6	127.6	56.7
19	1116	-109.4	1.1	355	-13.7	194.3	-3	129.5	47.6
20	1119	-106.7	2.7	0	-12.4	193	14	114	11.1
21	1122	-101.6	0.5	25	-13.9	214.8	2	131.2	30.3
22	1125	-150	5.6	12	-13.3	188.5	20	113	14.4
23	1128	-148	1.4	4	-15.4	209.1	13	124.8	47.1
24	1132	-152	4.3	352	-15.5	196.5	15	123.3	22.3
25	1370	-125.3	5.2	6	-12.2	190.4	29	126	23.5
26	1373	-127.5	4.9	359	-13.2	195.3	0	130.4	52.8
27	1376	-125.1	5.2	11	-14.3	207.6	7	125.9	63.6
28	1380	-133.4	4.2	7	-11.2	224.5	9	131.2	67.3
29	1385	-135.9	3.9	14	-10.5	169.3	21	137	49.7
30	1389	-145.6	4.2	18	-10.2	205.7	20	131.6	53.7
31	1391	-151.6	5.5	355	-13.2	210.2	34	118.3	1.8
32	1394	-155.7	3.6	359	-18.5	179.9	14	120.8	6.6

5.2 Directional PDP, Omni-directional PDP and corresponding AoD and AoA

Twenty rounds of simulation were conducted to calculate the Power delay profiles (PDP). In each round, the PDP for 10 transmitter-receiver locations, were calculated. This covers distances ranging from 50m to 500m and using different antenna configurations (16x1, 32x4, 64x8). Key parameters for each of the directional PDPs are calculated and presented in table 4. This includes time delay, received power, phase, azimuth and elevation AoDs and AoAs of each resolvable MPC (i.e., antenna pointing angle), along with directional path loss and directional R.M.S delay spread. Some of the data in Table 4 are presented in figure 2 which shows a sample of directional PDP with strongest power for 32x4 (32 Tx antenna and 4 Rx antenna) with 300 m distance separation between Tx and Rx using 28GHz frequency band. In the legend of figure (2), σ_τ represents R.M.S delay spread, P_r represents the strongest received power; PL represents the path loss, PLE represents the path loss exponent. As shown from table 4 and figure (2) there are 32 beams generated by Tx (As transmitter has 32 antennas) and these are grouped by 4 clusters at the receiver (as receiver has 4 antenna). The strongest received power is -33.6 dBm and the corresponding path loss is 113.4dB, R.M.S delay spread is 2.3 ns and PLE is 2.1 which is near PLE for free space (PLE =2 in free space).

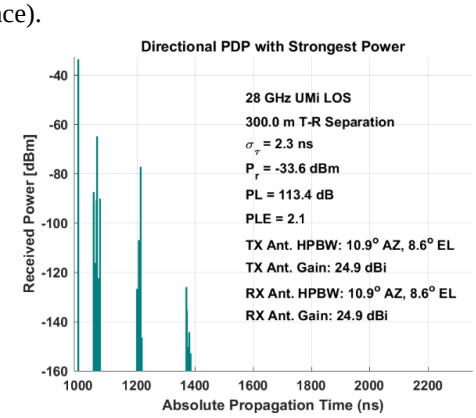

Figure 2. Directional PDP for 32X4 LOS 28GHz

It is worth to be noted that the directed PDP is generated by letting users to apply random directional antenna patterns (gains, and Half power Beam Width (HPBWs)) in an omnidirectional PDP. This is because in a realistic mmWave communication system, directional antenna arrays will be used at the transmitter and / or receiver to provide gains to pay compensation for the higher free space path loss at mmWave frequencies. The simulator then obtain the directional PDP by searching for the best pointing angle out of all possible pointing angles from the generated omnidirectional PDP by finding the pointing angle of the Tx and Rx that gives the strongest received power. The Tx/Rx antenna gain pattern is computed employing the azimuth and elevation HPBWs of Tx and Rx antennas using antenna pattern employed in [16]:

$$G(\theta,\emptyset) = \max(G_0\, e^{-\alpha\theta^2-\beta\emptyset^2}, \frac{G_0}{100}) \qquad (8)$$

$$\alpha = \frac{4ln\,(2)}{\theta_{3dB}^2}, \beta = \frac{4\ln(2)}{\emptyset_{3dB}^2}, G_0 = \frac{412\gamma 53}{\theta_{3dB}\emptyset_{3dB}}$$

where $(\theta,\emptyset)$ denote the azimuth and elevation angle offsets from the boresight direction in degrees, G_0 is the maximum directive gain (boresight gain) in linear units, (θ_{3dB} ; $\emptyset_{3dB}$) represent the azimuth and elevation HPBWs in degrees, (α; β) are parameters that depend on the HPBW values, and $\gamma = 0.7$ is a typical average antenna efficiency.

Figure (3) shows the normalized marginal power spectrum in the AoA domain consisting of 32 subpaths generated for 32x4 MIMO using LOS scenario, ULA antenna for 28 GHz band and with T-R distance =300m. It is shown from the figure that the strongest power beams fall within -2.5^0 to 2.5^0 with a peak beam of -33.6 dBm at 0.8^0, which indicates good MIMO directivity. Other weak beams are spread between -30^0 to 20^0.

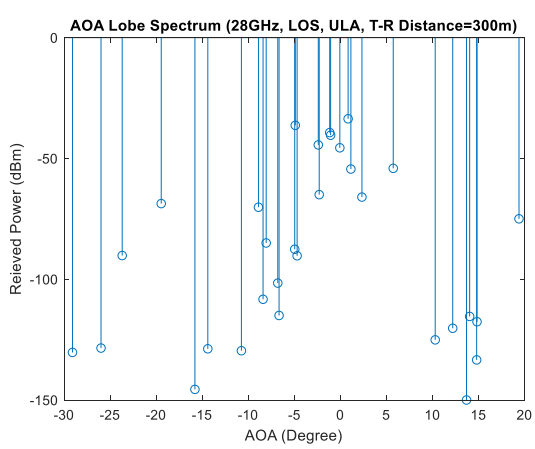

Figure 3. Normalized marginal power spectrum in the AoA domain

Figure (4) shows a sample of directional PDP for the same antenna configuration presented in figure (2) using 73 GHz frequency band.

Comparing figure (2) and (4), following remarks are extracted:

- The strongest received power in case of 28 GHz frequency was -33.6 dBm with path loss of 111.3 dB. For 73 GHz, the strongest received power was -40.9 dBm with path loss of 120.7 dB.
- R.M.S delay spreads for the strongest received power is equal to 2.3 ns for 28 GHz and 0.9 ns for 73GHZ band. The R.M.S delay spread is the root-mean-square value of the delay of reflections, weighted proportional to the energy in the reflected waves. The significance of the delay spread is how it affects the Inter Symbol Interference (ISI) and knowing the delay spread accurately is important in preventing ISI. ISI can be prevented either by using a guard band known as Cyclic Prefix (CP) with duration equal to delay spread inserted between LTE symbols. ISI also can be prevented if the symbol duration is made 10 times the delay spread. In this case, equivalent ISI-free channel is expected. Such channel is said to have Coherence bandwidth and is considered as a flat channel. The shorter the delay spread, the larger the coherence bandwidth. In our investigation, the 73 GHz band has shorter R.M.S delay spread as compared with 28 GHz.

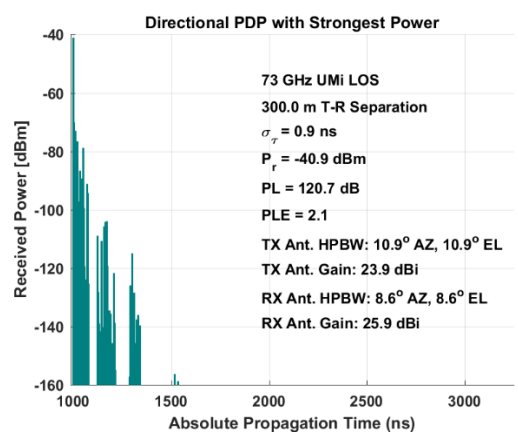

Figure 4. Directional PDP for 32x4 LOS 73GHz

- Most of the RF power was contained in multipath components arriving within 1100 ns

Figure (5) illustrates an omnidirectional PDP for 32x4 antenna, 28 GHz UMi, LOS for Tx-Tr= 300m. From Figure (5), the R.M.S delay is 16.8 ns which is more than the case of directional PDP. This is due to multipath effect as the delay spread is a measure of the multipath richness of a communications channel.

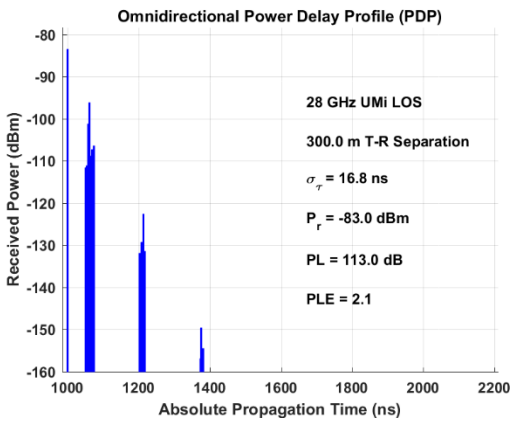

Figure 5. Omni-directional PDP

5.3 Path Loss

Path loss (PL) and path loss exponent (PLE) are important parameters that influence the quality of the link. These parameters if accurately calculated lead to efficient design and operation of wireless networks. Path Loss models are commonly used to estimate link budgets, cell sizes and shapes, capacity, handoff criteria etc. The value of PLE determines how quickly the Received Signal Strength (RSS) falls with distance. They are also significant in considering other issues in communications such as localization, energy-efficient routing, and channel access. Figures (6) and (7) show the calculated path loss for 28 GHz and 73 GHz frequency bands. In generating these figures, the Tx and Rx antenna azimuth and elevation HPBWs are set to 10.9o and 8.6o, respectively for LOS antenna and for NLOS antenna azimuth and elevation HPBWs are set to 7o as was used in [14-15]. The values in these figures are generated from 100 continuous simulation runs over a distance range of 50m to 500m. In addition to path loss, the fitted Path Loss Exponent (PLE) and shadow fading standard deviation are calculated using the minimum-mean-square-error (MMSE) method [14-15]. In Figures (6), (7), n denotes the PLE, σ_{omni} , σ_{dir} , $\sigma_{dir\text{-}best}$ is the shadow fading standard deviation, ”omni” denotes omnidirectional, ”dir.” represents directional, and ”dir-best” means the direction with the strongest received power. When comparing figure (6) and figure (7), following information are extracted:

- Generally, the path loss for 73 GHz frequency band is more than that of 28 GHz. This is clear as path loss is proportional to frequency as stated by equation (5) and (6) in section 4.1. As path loss is varying with distance, it is shown that at a distance of 100m path loss is higher with a magnitude of about 10dB.
- As shown in the figures, the directional path loss and directional PLE are lossier than the omnidirectional case. This is because the directional antenna will spatially filter out many MPCs due to its directional pattern, such that the Rx receives fewer MPCs hence less energy, thereby the directional path loss is higher after removing the antenna gain effect from the received power [13], [18].
- However, in figures (6) and (7), the calculated directional path loss exponents are calculated considering arbitrary unique pointing angles, but when searching for the strongest Tx-Rx angle pointing link at each Rx location it was decreased from 2.9 to 2.1 ($\sigma_{dir\text{-}best}$ in figure 6). This shows great significance of beamforming at the base station and mobile handset for SNR enhancement and increasing the coverage distance.

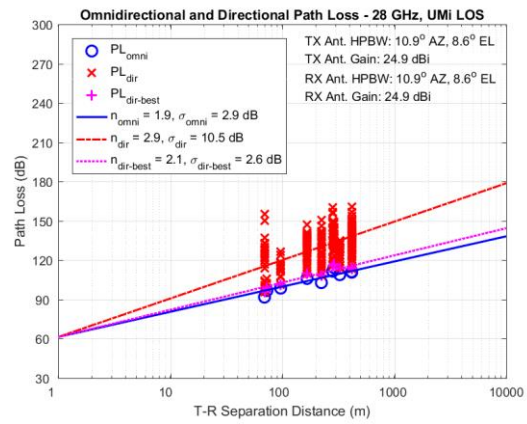

Figure 6. Path loss for 28GHz band (LOS)

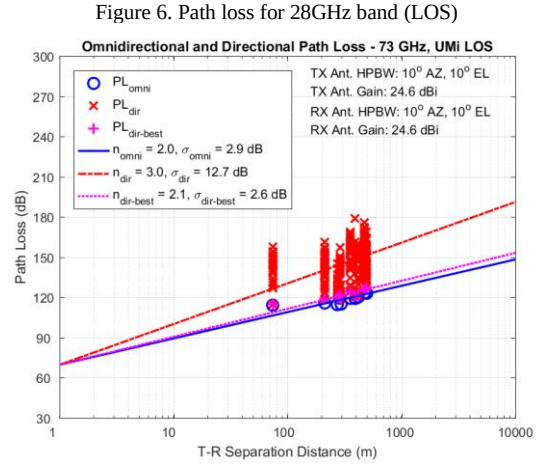

Figure 7. Path loss for 73GHz (LOS)

5.4 Antenna Array Effect

Antenna arrays are generally divided into separate types and have different properties and performance. The most common ones are Uniform Linear Array (ULA), Uniform Rectangular Array (URA) and Uniform Circular Array (UCA). In this paper, ULA and URA arrays are investigated and UCA array are left for future work. Figure (8) shows the received power using ULA and URL antenna arrays. It is shown from the figure that the URA antenna gives better performance than ULA antenna of about 4 dBm on average. The URA antenna used in the simulation consists of squared identical antenna elements, which are arranged, in an

equally spaced grid. Therefore, a URA is capable of resolving the angles of incoming wave fronts in azimuth and elevation thus we will have wider bandwidth and more angular spread. This shows improvement by 4 dBm achieved by URA antenna over ULA antenna.

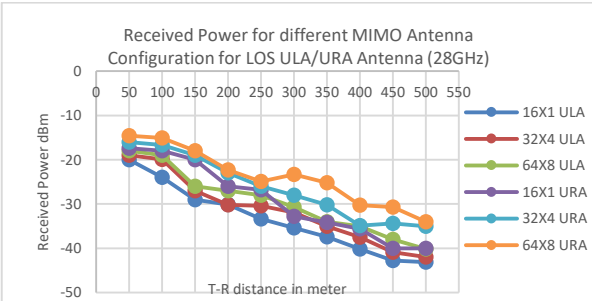

Figure 8. The received power using two types of antenna (ULA and URL)

5.5 LOS Vs. NLOS Transmission

Figure (9) shows the received power using LOS ULA/URA antenna and figure (10) shows the received power using NLOS ULA /URA antenna. It is shown from these figures that LOS gives better received power, as the power is concentrated in one direction rather than distributing the same power in many directions. However, in LOS antenna the transmitted power needs to be directed to the receiver using beamforming techniques to steer the beam to the dominant path at the transmit and receive ends by searching for the strongest Tx-Rx angle pointing link at each Rx location.

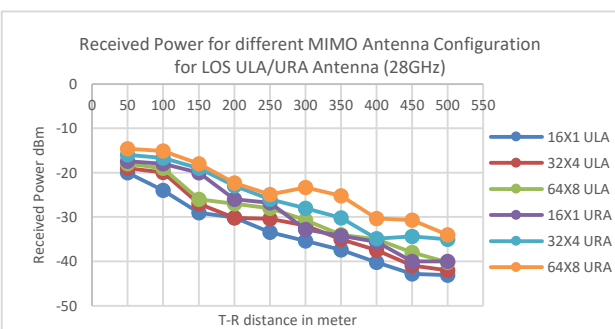

Figure 9. The received power using LOS ULA/URA antenna

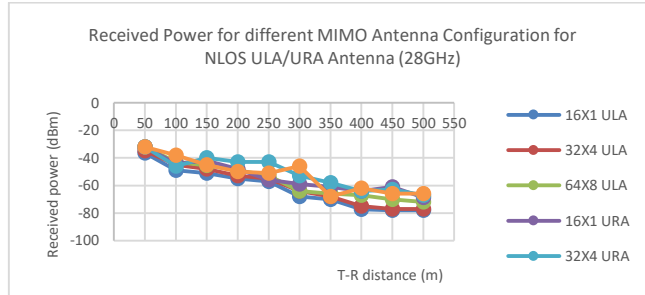

Figure 10. The received power using NLOS ULA /URA antenna

5.6 The effect of massive antenna

Figure (11) shows the received power for different antenna configurations (16X1, 32X4 and 64X8) using 28 GHz LOS scenario. It is shown from the figure that as the number of antennas increases, the received power (in dBm) becomes better. Using many antennas separated at certain distance from each other make each antenna to receive a slightly different version of the signal sent by the transmitter. The receiver combines them to form a better estimate of the transmitted signal as compared with the case of one receiving antenna. Moreover, with the increase in the number of BS antennas, the random channel vectors between the users and the base station become pair wisely orthogonal. Uncorrelated noise and intracell interference can be removed completely with simple matched filtering techniques. When increasing the antennas in Tx/Rx from 16x1 to 64x8, the array gain, in general should become 6 dBm better in Tx and 9 dBm in Rx which would make 15 dBm in total. However, as shown in figure (13) an average increase in performance of about 7dB has been achieved. This “only 7dB” gain increase partly comes from the directivity of the antenna when some of the paths are naturally being lost.

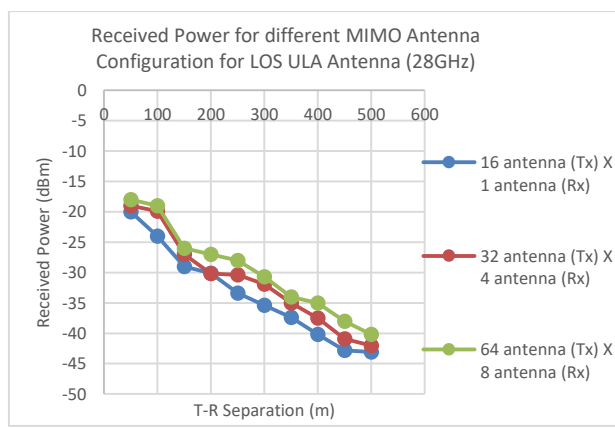

Figure 11. Effect of increasing number of antenna at Tx and Rx

6. MAIN FINDING

Investigation has shown that the coverage distances of the new frequencies for most of the cases can be good within a distance of 500m if a suitable transmitting power (about 30dBm) is used at the transmitter site. Path loss increases for these new bands and more dense cells are suitable to compensate for this extra path loss. For a distance of 100m, the path loss for 73 GHz is reported to be more than 28 GHz by an amount of 10 dB. Directional and Omni-directional PDP and R.M.S delay spread are calculated. These parameters are necessary for understanding inter-symbol interference (ISI) effects of the channel that could cause heavy data loss in communications especially in faded channels. The shorter the delay spread, the larger is the coherence bandwidth, and in our investigation the 73 GHz band has shorter R.M.S delay spread as compared with 28 GHz. It was shown that the directional path loss and directional PLE are lossier than the omnidirectional case as the directional antenna will spatially filter out many MPCs due to its directional pattern. This shows the significance of beamforming at the base station and mobile handset for SNR enhancement and increasing the coverage distance. In investigating the LOS and NLOS case, it was shown that LOS gives better received power, as the power is concentrated in one direction rather than distributing the same power in many directions. The comparison between ULA and URA antennas shows the URA antenna gives better performance than ULA antenna of about 4 dBm on average as URA is capable of resolving the angles of incoming wave fronts in azimuth and elevation and has more angular spread. This feature makes the URA more effective than ULA antenna.

7. CONCLUSION

As the race toward 5G networks intensify, the wireless spectrum below 6 GHz will not be enough to meet future 5G network needs. Several mmWave bands are currently being considered for global 5G networks. In this paper, the performance of Multiple Input Multiple Output (MIMO) systems for 28 GHz and 73 GHz frequency bands for outdoor communications are investigated to check their relevance for 5G. The investigation showed that these frequencies have good coverage distance, reasonable path loss, short R.M.S delay spread which lead to large coherence bandwidth. There are slight differences in coverage distance, path loss and other parameters between the 28GHz and 73GHz but in general, the two frequencies are suitable for the new 5G system. The study also compared the performance of different antenna types mainly ULA and URA and the investigation showed that URA antena has better performance. It was also shown that LOS has better received power than NLOS communication. The investigation of 28 GHz and 73 GHz frequencies presented in this paper will be helpful in understanding the mmWave system-wide behavior and radio-system design in outdoor environments for next generation 5G communication systems. As a future work, more simulations is need to investigate more characteristics of the new mmWave using different channel models like 3GPP, other types of antenna and different propagation scenarios.

REFERENCES

[1] Ant_onio Morgado, Kazi Mohammed Saidul Huq, Shahid Mumtaz *, Jonathan Rodriguez, “A survey of 5G technologies: regulatory, standardization and industrial perspectives, Digital Communications and Networks, Vol. 4, pp. 87–97, 2018. https://doi.org/10.1016/j.dcan.2017.09.010

[2] E. Dahlman, G. Mildh, S. Parkvall, J. Peisa, J. Sachs, and Y. Selén,"5G radio access," Ericsson review, vol. 91, pp. 42-48, 2014.

[3] FCC News, “FCC takes steps to facilitate mobile broadband and next generation wireless technologies in spectrum above 24 GHz,”; http://transition.fcc.gov/Daily_Releases/Daily_Business/2016/db0 714/DOC 340301A1.pdf (accessed on 2/1/2018).

[4] ITU-R, “IMT Vision – Framework and overall objectives of the future development of IMT for 2020 and beyond”. Sep. 2015, Recommendation M. 2083-0.

[5] 3GPP TR22.891, “Study on New Services and Markets Technology Enabler”. Sep. 2016, V14.2.0.

[6] Alauddin Al-Omary, “ Performance Evaluation of 28 and 73 GHz Ultra High Frequency Bands for Outdoor MIMO”, ”, International Conference on Cyber Security and Computer Science (ICONCS’18), Safranbolu, Turkey, Oct 18-20.

[7] Z. Pi and F. Khan, "An introduction to millimeter-wave mobile broadband systems," IEEE Commun. Mag. June 2011 49(6), 101-107.

[8] S. Rangan, T.S. Rappaport, E. Erkip, “Millimeter-wave Cellular Wireless Networks: Potentials and Challenges.” Proc. IEEE. Mar. 2014, 102 (3), 366-385.

[9] T. Bai, A. Alkhateeb, R.W. Heath, “Coverage and capacity of millimeter-wave cellular networks,” IEEE Commun. Mag. Sep. 2014, 52(9), 70-77.

[10] K. Sakaguchi, G.K. Tran, H. Shimodaira, S. Nanba, T. Sakurai, K. Takinami, I. Siaud, E.C. Strinati, A. Capone, I. Karls, R. Arefi, and T. Haustein, “Millimeter-wave Evolution for 5G Cellular Networks,” IEICE Trans. Commun. Mar. 2015, E98-B(3), 338- 402,.

[11] P. Soma, Y. Chia, and L. Ong, “Modeling and analysis of time varying radio propagation channel for lmds,” in 2000 IEEE Radio and Wireless Conference (RAWCON 2000). 2000, pp. 115–118.

[12] S. Geng, J. Kivinen, X. Zhao, and P. Vainikainen, “Millimeter-wave propagation channel characterization for short-range wireless communications,” IEEE Transactions on Vehicular Technology, Jan 2009, 58(1), 3–13.

[13] T. S. Rappaport et al., “Millimeter wave mobile communications for 5G cellular: It will work!” IEEE Access. May 2013, 1,335–349.

[14] _____, 5G Channel Model for bands up to 100 GHz. March 2016. http://www.5gworkshops.com/5G_Channel_Model_for_bands_up_to100_GHz(2015-12-6).pdf (accessed on 3/2/2018)

[15] M. K. Samimi and T. S. Rappaport, "3-D millimeter-wave statistical channel model for 5G wireless system design," IEEE Transactions on Microwave Theory and Techniques. July, 2016, 64(7), 2207–2225.

[16] M. K. Samimi, T. S. Rappaport, and G. R. MacCartney, Jr., "Probabilistic omnidirectional path loss models for millimeter-wave outdoor communications," in IEEE Wireless Communications Letters. Aug. 2015, 4(4), 357–360.

[17] M. K. Samimi and T. S. Rappaport, "Ultra-wideband statistical channel model for non-line of sight millimeter-wave urban channels," in 2014 IEEE Global Communications Conference (GLOBECOM). Dec. 2014, 3483–3489.

[18] M. K. Samimi and T. S. Rappaport, "Statistical Channel Model with Multi-Frequency and Arbitrary Antenna Beamwidth for Millimeter-Wave Outdoor Communications," in 2015 IEEE Global Communications Conference (GLOBECOM) Workshop. Dec. 2015, 1-7.

[19] M. Steinbauer, A. F. Molisch, and E. Bonek, "The double-directional radio channel," IEEE Antennas Propag. Mag. Aug. 2001, 43(4), 51–63.

[20] T. S. Rappaport et al., "Wideband millimeter-wave propagation measurements and channel models for future wireless communication system design (Invited Paper)," IEEE Transactions on Communications. Sep. 2015, 63(9), 3029–3056.

[21] S. Sun et al., "Investigation of prediction accuracy, sensitivity, and parameter stability of large-scale propagation path loss models for 5G wireless communications," IEEE Transactions on Vehicular Technology. May 2016, 65(5), 2843–2860.

[22] T. S. Rappaport, R. W. Heath, Jr., R. C. Daniels, and J. N. Murdock, Millimeter Wave Wireless Communications. 2015, Pearson/Prentice Hall.

[23] G. R. MacCartney, Jr. et al., "Indoor office wideband millimeter-wave propagation measurements and channel models at 28 and 73 GHz for ultra-dense 5G wireless networks," IEEE Access. Oct. 2015, 3, 2388–2424.

[24] S. Sun, G. R. MacCartney Jr., and T. S. Rappaport," A novel millimeter-wave channel simulator and applications for 5G wireless communications," 2017 IEEE International Conference on Communications (ICC). May 2017, 1-4, DOI: 10.1109/ICC.2017.7996792.

Alauddin Al-Omary Holds M.Sc. in Communication Engineering and PhD in system and information engineering from Toyohashi University, Japan, 1994. Since 2005, he is an associate professor at the Department of Computer Engineering, College of Information Technology, University of Bahrain. His research interests include Hardware/Software co-design Telematics system, Mobile Network performance, ASIC and embedded system design using VHDL and FPGA. He has been actively involved in many research projects and published 2 books and more than 60 papers. He is a member of the Institute of Electrical and Electronic Engineers (IEEE), the Japanese Information Processing Society and the International Association of Computer Science and Information Technology (IACSIT), He was a Member of the UNESCO Project to establish a computer networks between the GCC's Inheritance and folklore centers started in April 2001 until April 2002. Dr. Al-Omary is the founder of the International Journal of Computing and Network technology (IJCNT).